# Development of a Reactive Sulfate Transport Model for a Minnesota Taconite Tailings Basin (Minntac)

**G.-H. Crystal Ng, Patrick O'Hara, and Amanda Yourd**

**Department of Earth Sciences, University of Minnesota, Twin Cities**

**Final Draft Submitted to Minnesota Department of Natural Resources**
**11/23/16**

## Abstract

Mining-derived sulfate has become an issue of growing concern on the Iron Range in northeastern Minnesota where tailings basins have been identified as potentially important sulfate sources. At the Minntac tailings basin in Mountain Iron, MN, elevated sulfate has been observed in both surface water and groundwater beyond the outer perimeter of the basin. Process water contained within the tailings basin has elevated sulfate, and this water is released via groundwater through and below the basin's perimeter dike, but dilution, pyrite oxidation, and sulfate reduction have all been found to occur at this basin and affect final concentrations and loading outside the basin.

This study furthers our understanding of sulfate transport at U.S. Steel Minntac's tailings basin by developing reactive transport models for six representative cross sections across the Minntac tailings basin's outer perimeter dike. The models were constructed using a variety of available hydrologic and geochemical observations, which served as both model inputs and calibration targets. Measured chloride concentrations were used to constrain dilution, and measured sulfate release rates were used to constrain oxidation of pyrite in the perimeter dike. The resulting models demonstrate that basin water serves as the largest sulfate source in nearly all of the cross sections, while additional sulfate loading with precipitation-related recharge depends on the specific hydraulic conditions of the particular cross section. Sulfate concentrations attenuate as groundwater leaves the dike, due to both dilution from recharge through naturally vegetated land and due to sulfate reduction and precipitation of iron sulfide minerals. How much sulfate reduction occurs depends on organic carbon reactivity as well as groundwater velocities for a particular cross section. However, in nearly all cross sections, the majority of sulfate leaves the system at the down-gradient end of the cross section rather than reducing along the flow path.

The biggest sources of uncertainty for the model consist of lack of data in the west side of the Minntac tailings basin, insufficient information about subsurface heterogeneity, and poor constraints on mechanisms controlling organic carbon degradation and sulfate reduction. To address these issues and improve our understanding of sulfate release from the Minntac tailings basin, we recommend the following additional data collection and model developments: (1) installing west-side monitoring wells to provide hydrologic and geochemical observations; (2) collection of cores of the subsurface material to constrain spatial heterogeneity, geochemical sulfide sinks, and microbial properties; (3) incorporating cation exchange and major cations into the geochemical model as indicators of flow and redox processes; and (4) rigorously quantifying uncertainty in the model to understand its value and limitations for making future predictions. Reactive-transport models can play a critical role in evaluating future scenarios of sulfate release as Minntac's activities move forward and as site closure is planned, but a greater understanding of geochemical mechanisms and subsurface physical properties is first needed to reliably project sulfate reduction processes long into the future.

## Introduction

The release of dissolved sulfate into surface water is an issue of growing concern on the Iron Range in northeastern Minnesota. The sulfate is released via the oxidation of iron sulfide minerals such as pyrite in mine tailings and stock piles. Although iron sulfide minerals occur naturally in small amounts on the Iron Range, the mining process involves blasting and crushing of vast amounts of material, increasing freshly exposed surface area available for oxidation and sulfate release. The sulfate-rich waters initially pumped from the mineral processing plants are stored in large mine tailings basins, where they can seep into groundwater and surface water. Additional sulfate that is generated via oxidation of blasted rocks in mine pits mixes and contributes to sulfate in pit waters that are sumped into nearby streams.

If the sulfate moves into anoxic sediments, it can be geochemically reduced to sulfide, which is toxic to wild rice (*Zizania palustris*) in its dissolved form [MPCA, 2015]. Sulfate reduction has also been associated with methyl-mercury (MeHg) production [Branfireun et al. 1999; Harmon et al. 2004; Jeremiason et al. 2006], alkalinity increases, and phosphate release [Holmer and Storkholm, 2001]. However, reactions of dissolved sulfide with iron precipitate iron sulfide minerals, which can also help to attenuate both sulfide concentrations and its toxic effects in porewaters. Moreover, the combined effect of sulfate reduction and iron sulfide precipitation can help decrease the amount of sulfate that reaches surface waters. Thus, the State of Minnesota has been studying how sulfate is generated during mining and evaluating its transport and reduction as it is released from tailings basins [Berndt et al., 2016a and references there in].

This study, conducted on behalf of the Minnesota DNR, evaluates sulfate transport processes near the U.S. Steel Minntac tailings basin (Figure 1). The study's focus is on water that seeps through and beneath the outer perimeter dike into surrounding natural groundwater, which then discharges to surface waters. This dike is composed of tailings that contain small amounts of pyrite that can oxidize to sulfate when oxygenated water infiltrates [Berndt et al., 2016b; Kelly et al., 2016]. When this sulfate encounters naturally occurring organic carbon in the glacial till underlying the perimeter dike, it can be reduced to sulfide, which can then precipitate with iron to form iron sulfide minerals [Kelly et al., 2016]. This study attempts to link these physical and geochemical processes using the reactive transport model PHT3D [Prommer et al., 2003]. PHT3D pairs physical hydrologic conditions with geochemical processes to simulate reactive transport, and it is applied over a 12 year period in 6 different cross sections throughout the perimeter dike.

## Method Overview

The reactive transport model PHT3D [Prommer et al., 2003] was employed to investigate sulfate release via groundwater at six cross sections traversing the outer perimeter dike of the Minntac tailings basin. PHT3D combines the geochemical model PHREEQC-2 [Parkhurst and Appelo, 1999] with the transport model MT3DMS [Zheng and Wang, 1999], which incorporates flow results from the groundwater model MODFLOW [Harbaugh, 2005]. Cross sectional model domains on the east and west sides of the basin were established based on topographic and geological data provided by the Minnesota DNR and U.S. Steel Minntac. The generic model for each cross section begins at its hydraulically up-gradient end at the inner edge of the outer

perimeter dike and extends to the down-gradient end at a monitoring well located outside of the outer perimeter dike (Figure 2). The dike is comprised of relatively conductive coarse tailings with an inner core of relatively impermeable fine tailings. Natural till underlies the dike and extends down-gradient through the remainder of the domain. Steady-state flow is assumed based on observed and inferred hydraulic conditions.

For the geochemical component, boundary conditions include: (1) elevated concentrations of chloride and sulfate from basin water at the up-gradient end as measured in 2014 and 2015, (2) high recharge inputs of sulfate generated from iron sulfide oxidation in the dike, and (3) natural recharge water with negligible concentrations of chloride and sulfate down-gradient of the dike. Field measurements of hydrologic and geochemical properties were used as model inputs where they were available or could be reasonably assumed; water chemistry measurements (chloride and sulfate) at down-gradient monitoring wells served as calibration targets for constraining other model parameters. Within the model domains, sulfate and other solutes are transported via advection with the flow field and hydrodynamical dispersion. Sulfate concentrations are also controlled by reduction coupled to organic carbon oxidation in till, which is supported by sulfur isotope data [Kelly et al., 2016]. Sulfide produced during sulfate reduction is allowed to precipitate with iron in the model based on the observed presence of high iron and negligible sulfide in well waters. The main parameters calibrated in this study include: hydraulic conductivity for different porous media types (coarse tailings, fine tailings, and till), hydraulic head in the west side of the basin, kinetic parameters for sulfate reduction, and organic carbon concentrations in till. The main processes represented in the model are shown in Figure 2. Details on the model development for each cross-section are described in the below sections.

## Site Description

The approximately 9 $mi^2$ Minntac tailings basin in Mountain Iron, MN can be seen in Figure 1. It is located just north of associated taconite mining pits. Its two main functions are to serve as a disposal site for tailings as well as a reservoir for process water from the processing plant located between the pits and basin. Within the tailings basin, there are a series of inner cells that are used as reservoirs for tailings, which are deposited as a slurry of finely ground gangue minerals mixed with processing water. Each inner cell is surrounded by a dike composed of coarse tails that provide support structure for the fine tails in the cell. Minntac cycles fine tailings deposition through the different inner cells over time. When cells are inactive, vegetation is established and helps prevent wind erosion.

The outer edge of the tailings basin consists of a perimeter dike built on pre-existing glacial till; the dike is constructed mainly with coarse tailings but also contains an inner fine tails portion keyed in approximately 10 ft below the ground surface. Between the outer perimeter dike and the inner cells on the west side, a surface stream has developed and flows clock-wise along the perimeter dike until reaching a series of reservoir ponds holding process water. This water is recycled by Minntac for the taconite extraction process. The two major reservoir ponds on the east side of the basin are referred to as Cells 1 (south) and 2 (north) (Figure 1).

Six representative cross sections traversing the outer perimeter dike (Figure 1) were the focus of this modeling study. Each cross-section is identified by the monitoring wells at the hydraulic

down-gradient end: GW003, GW004, GW006, GW007, GW008 and MW12. The southern pond "Cell 1" on the east side of the basin is the up-gradient boundary of the GW003 cross-section. Also on the east side, GW004 and MW12 cross-sections have Cell 2 as their up-gradient boundary. Cross-sections GW006, GW007 and GW008 are on the west side of the tailings basin, where there are no surface water reservoirs to serve as convenient groundwater boundaries; other information was used to constrain gradients for those cross sections.

## Data

### Physical Data

Hydraulic head was measured once in 2012 and three times in 2014 at each of the monitoring wells at the down-gradient end of each cross section [MN DNR, unpublished data]. Head values averaged over the observational period are used for steady-state flow modeling and are listed in Table 1. Cell 1 and 2 water levels that were used in the model were measured weekly starting in January 2011 and ending in December of 2012 [U. S. Steel, unpublished data, 2016]. Average values over the observational period serve as up-gradient head boundary conditions for east-side transects and are listed in Table 1. An additional piezometer was located a few meters south of the GW007 transect within the tailings basin. The average of two static water level measurements taken in the spring and summer of 2016 served as the up-gradient head level for GW007 (Table 1) [T. Moe (U.S. Steel), personal communication, July 2016].

Recharge rates were taken from the MNDNR report by Bavin et al. [2016] and are listed in Table 2. There are two recharge rates, a higher one for recharge through the perimeter dike, where there is little to no transpiration, and the other for recharge rates below naturally vegetated land surface.

Hydraulic conductivities for the fine and coarse tailings are averages of values found from slug tests conducted by STS [2007]. Hydraulic conductivity for the underlying till is more heterogeneous due to natural variability. Slug tests by STS [2007] and slug tests and pumping tests by CRA [2013] were used to bracket the range of possible hydraulic conductivity values for till. Ranges of observed hydraulic conductivity values for all of the porous media types are listed in Table 3.

### Geochemical Data

Our model incorporates data collected at the Minntac tailings basin, including water chemistry and temperature measured twice in 2014 and once in 2015 at each monitoring well [Kelly et al, 2016] and five times each for water in Cells 1 and 2 [Berndt et al., 2016a]. Time-averaged values of temperature and at each monitoring well (Table 4) were used to represent conditions within the corresponding cross-section. Time-averaged values of sulfate and chloride concentrations in Cells 1 and 2 (Table 5) are used to represent up-gradient boundary conditions. The observed ranges of sulfate and chloride concentrations at each monitoring wells provided important model calibration targets. Sulfate loading from iron sulfide oxidation in the dike was estimated to be

approximately 15 metric tons/mi$^2$/week using field-based rate measurement methods [Berndt et al. 2016b].

## Model Formulation

A series of reactive transport model implementations have been carried out to simulate the geochemical processes controlling sulfate release and evolution across 6 cross-sections at the Minntac tailings basin. We used the reactive transport model PHT3D [Prommer et al., 2003], which couples the physical transport model MT3DMS [Zheng and Wang, 1999] with the geochemical model PHREEQC-2 [Parkhurst and Appelo, 1999] model code; PHT3D inputs include groundwater flow fields generated using MODFLOW-2005.

### Model Domain and Groundwater Flow Model

A 2D steady-state flow field was simulated for each of the 6 cross-sections using MODFLOW-2005. For each cross-section, domain length was determined using LiDAR data available from MN DNR's MNTOPO website [DNR, 2016]. Transect lengths (Table 1) were calculated using known locations of monitoring wells and satellite imagery of the outer perimeter dike. Horizontal length of the outer perimeter dike was found using a combination of LiDAR data acquired from MNTOPO and satellite imagery. The base of the coarse tailings component of the perimeter dike was set to the elevation at which the natural land surface meets the outer end of the outer perimeter dike. The fine tailings, which make up the inner portion of the perimeter dike, were set an additional 10 ft below the base of the coarse tailings based on information found within a hydrogeological assessment by USS [1987]. Domain height of the transects were determined via a combination of surface elevation data acquired from MNTOPO and depth-to-bedrock information acquired through the Minnesota Geological Survey's "State Map Series" Map S-21 [MGS, 2016]. The distance from the surface to the relatively impermeable bedrock served as the initial domain height. Later, the top of the domain was set to the highest elevation of the water table within the cross-section.

Each cross-section was discretized into a grid consisting of 75 horizontal layers and 150 vertical columns. This level of discretization allows for proper representation of heterogeneity and transient dynamics while remaining coarse enough for computational tractability.

Four boundary conditions are required for each 2D cross-section. The up-gradient and down-gradient lateral boundaries were set as constant head boundaries and are listed in Table 1. Down-gradient head was set according to monitoring well head measurements for all cross-sections. Time-averaged pond levels in Cells 1 and 2 were applied as constant up-gradient head boundary conditions at the dike on the east side (Cell 1 for GW003 and MW12 and Cell 2 for GW004). Variable up-gradient head was allowed for grid cells below the dike, which are presumably below the bottom of the pond water. On the west side of the basin, the up-gradient head level for GW007 was taken from head measurements at a nearby piezometer. The up-gradient head levels for GW006 and GW008 were inferred based on hydraulic conductivity values calibrated at GW007 (discussed further below).

The upper boundaries for all models were set as constant flow boundaries corresponding to recharge rates in Table 2. The higher recharge rates are applied over the locations corresponding to the perimeter dike, while the lower natural recharge rate is applied to locations down-gradient of the dike. The bottom no-flow boundary condition represents the relatively impermeable bedrock. Depth to bedrock was determined using bedrock data acquired from the Minnesota Geological Survey's "State Map Series" Map S-21 [MGS, 2016].

Although in theory, initial head conditions are not needed to calculate steady-state groundwater conditions, MODFLOW takes user-specified initial head values as the starting point for its numerical iterative solver. We generated an initial head field that follows a constant horizontal gradient from the up-gradient head value to the down-gradient head value.

All cross-sections used the same average fine and coarse tailings hydraulic conductivities summarized in Table 1. Because of the natural heterogeneity of till, we calibrated unique hydraulic conductivity values for each cross-section within the observed range indicated in Table 3. After setting hydraulic gradient and recharge fluxes based on measurements, hydraulic conductivity for till was adjusted for GW003, GW004, GW007 and MW12 to match measurements of the conservative tracer chloride at the down-gradient monitoring well. Because there are no available up-gradient head measurements for GW006 and GW008, till hydraulic conductivity for GW007 was applied based on proximity. Up-gradient head measurements at GW006 and GW008 were then further calibrated based on measured chloride at the monitoring well.

The resulting steady-state flow fields for each cross-section were used as input for the transport component of PHT3D. Porosity at all cross-sections was fixed to 0.35 based on a range of measured values taken from the MNDNR report by Bavin et al. [2016].

**Geochemical Model**

The model includes the following aqueous components: inorganic carbon, chloride, iron, sodium, sulfur, dissolved oxygen, and pH. It also includes sorbed labile organic carbon (OC), siderite ($FeCO_3$), and iron sulfide minerals. Chloride is not involved in geochemical transformations and is thus used as a conservative tracer of physical transport. Organic carbon degradation drives redox reactions that can involve dissolved oxygen respiration and sulfate reduction to sulfide; to simplify the redox relationships, iron(III) oxide minerals are not included in the model to exclude competition by iron reduction. The role of iron comes into the model through an initial reservoir of siderite, which provides a source of iron(II) that can react with sulfide to precipitate iron sulfide. pH is involved in redox and mineral phase reactions, and these relationships, along with other equilibrium processes, such as reoxidation of sulfide and iron(II), are incorporated through the default PHT3D geochemical database. Sodium is not considered an important analyte in this study and is allowed to adjust in the model to maintain charge balance.

Simulations follow the partial equilibrium approach of Jakobsen and Potsma [1999], in which redox reactions are controlled by the availability of electron donors, most commonly present as

various forms of labile organic carbon. Following this approach, the oxidation half of the redox reaction (organic carbon degradation) is kinetic, while the reduction half of the reaction is assumed to be at or near equilibrium. In other words, kinetic organic carbon degradation rate is linked to equilibrium sulfate and iron reduction as the limiting reactant.

Kinetic degradation of organic carbon is assumed to follow a first-order rate relative to the organic carbon concentration: $d[OC]/dt = -k[OC]$, with the decay parameter k. The model uses a higher aerobic decay parameter of $1x10^{-7}s^{-1}$ and lower anaerobic decay parameter of $7.5x10^{-8}s^{-1}$ to reflect the efficiency differences between the two types of microbially mediated degradation. These kinetic parameters were adjusted along with organic carbon concentrations to match observed sulfate concentrations. The same kinetic parameters were applied at all cross section based on assumed similarities among microbial behavior within the study area.

The model domain geochemistry is initialized uniformly with idealized background conditions that include reservoirs of labile organic carbon sorbed to till sediments, iron minerals in the form of siderite, and no sulfate or chloride. PHREEQC-2 was used to equilibrate the initial aqueous concentrations with siderite and establish charge balance; results are shown in Table 6. The equilibrated concentration for sodium is unaturally high because it was used as a charge balance ion and compensates for the absence of other major cations such as $Ca^{2+}$ and $Mg^{2+}$ in the model. The equilibrated pH (7.1) and total dissolved inorganic carbon (0.035) are similar to average measurements from MW12 (pH = 7.1 and total dissolved inorganic carbon = 0.037 mM). Although elevated chloride and sulfate concentrations at all monitoring wells indicate that none are likely to represent background conditions, measurements from MW12 were chosen for comparison because it is located farthest outside the dike and provides some guideline for field conditions. Over a 12-year simulation period, the upgradient boundary releases a constant concentration solution representing oxygenated basin water with elevated concentrations of chloride and sulfate. For up-gradient boundary conditions, time-averaged solute concentrations measured in Cell 1 water were applied for GW003, and concentrations measured in Cell 2 were used for all remaining cross-sections (Table 5). Recharge through the dike is set to have a sulfate concentration of 0.0726 mg/L for all cross-sections, which corresponds to loading results reported by Berndt et al. [2016a]. Recharge below naturally vegetated land-surface areas down-gradient of the dike have negligible sulfate. All recharge waters are assumed to have negligible chloride.

Within the domain, tailings that make up the dike are primarily comprised of relatively fresh crushed rock and can be assumed to bear negligible organic matter. Exact organic carbon concentrations in the till are unknown, but because organic carbon degradation is linked to sulfate reduction, initial concentrations for each cross-section were calibrated such that simulations match measured sulfate at the corresponding monitoring well at the end of the simulation period. Calibrated initial organic carbon concentrations are listed in Table 7. An arbitrarily large concentration of siderite ($FeCO_3$) is specified in the initial conditions to provide a source of dissolved iron. Equilibrium FeS precipitation is included in the model to serves as a sink for S produced during $SO_4$ reduction.

Time-averaged temperature from each monitoring well locations vary between the cross sections (Table 4). For all cross-sections, tortuosity was set to 0.5 [Bear and Verruijt, 1987], the

molecular diffusion coefficient was set to $1.16x10^{-14}$ [Li and Gregory, 1974], longitudinal dispersivity was set to 1m [Gelhar et al., 1992], and horizontal and vertical ratios of transverse to longitudinal dispersivity were set to 0.018 and 0.0015, respectively [Garabedian, 1991].

## Results/Discussion

### Groundwater Flow

The spatial variability of hydraulic conductivity and the resulting flow lines and average groundwater velocities are shown in Figures 3a and 3b for the east and west cross-sections, respectively. Water balance discrepancies calculated by MODFLOW are shown in Table 8; most are within well within 1%, with only GW007 presenting a larger but moderate 1.19% difference. Average calibrated groundwater velocities for all cross-sections fall within the same order of magnitude, with GW007 on the west side having the slowest groundwater velocity (0.028 m/d) and GW003 on the east-side having the fastest groundwater velocity (0.074 m/d). Average groundwater velocities are generally greater on the east-side due to their higher hydraulic conductivities for till (Table 1), but hydraulic gradient is the other factor, which contributes to slower flow for MW004. Groundwater velocity may have a significant control on sulfate reduction; longer travel times through the subsurface provides more time for chemical processes leading to sulfate reduction to occur. This is discussed further in the Geochemical Results/Discussion section.

In general, the flow results are relatively similar in all cross-sections. One major similarity is how the inner-core of the perimeter dike, composed of fine tailings, diverts horizontal groundwater flow around it; flow lines bend downward below the inner-core and then move back upward beyond th core. The path of the flow lines through the different porous media types affects geochemical results, because organic carbon and, thus, sulfate reduction, only occurs in the till layer.

East side cross-sections GW003, GW004 and MW12 show variable flow lines from the up-gradient end due to the different head controls in the dike (set to cell water levels) versus the underlying till (set to variable head). In the up-gradient till, simulated downward flow is consistent with surface water system percolating downward into groundwater. Flow lines starting in the coarse tailings in the dike also exhibit an inflection at the till boundary, due to higher calibrated hydraulic conductivity in the till compared to the coarse tailings. In contrast, west side cross-sections GW006, GW007 and GW008 have calibrated till hydraulic conductivity values that are similar to coarse tailings and thus exhibit smoother flow line transitions from the coarse tailings to the till.

### Geochemistry

Chloride and sulfate geochemistry results at the end of the 12-year simulation periods for all 6 cross sections are shown in Figures 4a–4c. In all cross sections, the conservative tracer chloride increases with depth while recharge water dilutes the top of the domain. As a reactive redox species, sulfate trends are more variable between the cross sections. In general, sulfate

concentrations are higher near the top and up-gradient end than near the bottom and down-gradient end of the domain. The simulated range of pH across the different cross-sections (6.7 to 7.1) corresponds well with the average measured range at the 6 monitoring wells (6.4 to 6.9), lending confidence that the model generates reasonable pH-related redox reactions. Solute mass balance discrepancies reported by PHT3D for each cross-section are shown in Table 9. Most discrepancies are within 1%, although magnitudes as high as 4.56% occur, likely due to to known numerical difficulties in solving reactive advection-dispersion problems.

A comparison of simulated sulfate fluxes into and out of the cross sections are shown in Table 10. The near balance between sulfate sources and sinks indicates that GW006 has reached steady-state (with respect to sulfate) by the end of the 12-year simulation period (Table 10). The cross-section reaches steady-state when in-fluxes are balanced by out-fluxes, such that the chemistry within the domain does not change. With >5% discrepancies between total flux in and out, GW008 and, to a lesser degree, GW007, are still most prominently exhibiting transient changes still after 12 years. For these cross-sections, the sulfate front has yet to fully reach the down-gradient end of the domain. It should be noted, though, that all cross sections have reached steady-state for chloride concentrations.

Variability in sulfate results among the cross sections is due to differences in organic carbon, boundary fluxes, and hydraulic conductivity, each of which are linked to sources or sinks of sulfate. Discussion of how each of these three factors affect sulfate are included below. Simulated iron sulfide precipitate results are then described to illustrate how sulfate is reduced and then stored in minerals.

*Boundary Fluxes*

Boundary fluxes include in-flows from the basin (up-gradient end) and from recharge, and out-flow at the down-gradient end. Sulfate enters with recharge only through the dike, where infiltrating oxygenated water oxidizes iron sulfide in the tailings. Because all cross-sections are assumed to have the same recharge flux through the dike (Table 2) and recharge concentration (see above), differences in total sulfate loading through recharge arise only with variability in dike lengths in the cross sections. These lengths are similar around the basin perimeter, resulting in very similar total sulfate inputs with recharge (Table 10).

The basin contributes the largest input to the sulfate balance in nearly all the cross-sections. Up-gradient concentrations from the basin are very similar across cross sections (Table 5), but water flux rates vary considerably due to differences in hydraulic conditions and domain geometry. Sulfate flux from the basin is greatest for the east-side cross sections, which generally have higher groundwater flow velocities. The cross section GW008 has the lowest up-gradient flux of sulfate, due to lower flux magnitudes and a smaller vertical domain to receive sulfate from the basin.

For many of the cross sections, down-gradient out-flux of sulfate represents the largest sink. The exceptions are GW004 and GW008, both of which lose more sulfate to reduction. Once the domain reaches geochemical steady state, the out-flux will include the balance of sulfate that

reaches the down-gradient end after reduction processes, which are determined by organic carbon concentrations and flow path within the domain.

*Organic Carbon*

Sediment organic carbon was used as a calibration parameter for each of the cross sections, based on the partial equilibrium assumption that higher organic carbon concentrations lead to higher rates of sulfate reduction through redox coupling [Jakobsen and Potsma, 1999]. Because of unavailable field measurements and high natural variability of organic carbon in glacial till, organic carbon concentrations were initially set at low concentrations ($2.1x10^{-5}$ mol/L) for each cross section and increased until sulfate reduction was sufficient to match down-gradient measurements of sulfate at the monitoring wells. Once down-gradient sulfate concentrations were matched, organic carbon was held constant at the calibrated value (Table 7) over the simulation period. With a pre-set first-order degradation coefficient (see the above "Geochemical Model" description), this is equivalent to calibrating a constant redox rate, which follows the assumption that the organic carbon reservoir in the till is sufficiently plentiful that it does not deplete to appreciably limit kinetic processes. Sulfide generated due to sulfate reduction precipitates out with locally available iron, functionally decreasing sulfate and "locking up" sulfide in the sediments. Because of this process, organic carbon can also be thought of as proxy sink for sulfate.

The trend of organic carbon removing sulfate is especially clear in cross sections with the highest organic carbon levels (GW004, GW003, GW008). The high sediment organic carbon produces simulations that match the relatively low down-gradient sulfate levels observed and result in some of the highest rates of sulfate reduction (Table 10). Note that somewhat lower concentration of organic carbon for MW12 (about 25% lower than GW003 and GW008) also produces a similarly significant amount of sulfate reduction, but this is due to the much longer domain containing greater till area. Cross sections with lowest organic carbon concentrations (GW006, GW007) allow simulation of higher down-gradient sulfate levels, as observed (Figure 4b). In fact, organic carbon concentrations in GW006 and GW007 are so low that negligible sulfate reduction occurs in those cross sections (Table 10).

*Flux within the Domain*

In all cross sections, hydraulic conductivity is much lower in the fine tailings than in the coarse tailings and till, and the physical flow results show little to no horizontal groundwater flow through the inner core of the dike. High sulfate concentrations are observed in the fine tailings section due to loading from recharge water through the dike. This sulfate-rich water does not readily flow through the poorly conductive fine tailings, allowing sulfate to accumulate in this area. As noted above, the sulfate concentrations have not yet reached steady-state by 12 years for most of the cross sections other than GW006, which is reflected in sulfate fronts not yet reaching the base of the fine tailings section in many of those cross sections. Travel time of the

sulfate front through the fine tailings section also depends on the depth of fine tailings below the water table.

As noted during discussion of groundwater flow results, cross sections with slower groundwater velocities allow greater residence time of groundwater sulfate in organic carbon-bearing till sediments, facilitating sulfate reduction. Although GW003 and GW008 cross sections include similar organic carbon concentrations, slower groundwater velocity in GW008 (Figure 3b) cause very sharp sulfate gradients in the till below dike, as much of the sulfate is reduced before advecting down-gradient. Note that total sulfate reduction in the domain is greater in GW003 compared to GW008, but this is also due to differences in groundwater velocities, with higher sulfate transport rates in GW003 facilitating greater areas of sulfate reduction.

*Iron sulfide precipitation*

Total dissolved sulfide concentrations in the wells are low but detectable using sensitive techniques. In October 2012, the Minnesota DNR analyzed sulfide in six wells and found concentrations to range from approximately 0.03 to 0.10 mg/l (MnDNR unpublished data). These very low concentrations are not surprising, because iron concentrations tend to be high, meaning that any sulfide formed should precipitate out of the groundwater as iron sulfide. Using a literature-based solubility for iron-sulfide precipitates (equilibrium mineral phase "FeS(ppt)" in the PHREEQC-2 database), the model simulated precipitation of nearly all sulfide generated through sulfate reduction in the till (Table 10). Thus, even though no efforts have been made to quantify the amount of iron sulfide in or around the Minntac basin, model simulations support the possibility it forming.

## Model Uncertainty

Assessments of the model can be made by comparing simulations with direct observations and other data from the Minntac basin. Discrepancies between the model and observations or other estimates can be attributed to uncertainty in either the model or the observations/estimates. Some model errors may be associated to measurements errors in model inputs, but most are likely associated with assumptions made when measurements were not available. Comparisons between simulated results and target observations provide a performance assessment, but non-uniqueness in the calibration approach is always a possible source of uncertainty.

The main calibration targets for organic carbon content and hydraulic conductivity were sulfate and chloride concentrations, respectively, at the down-gradient monitoring wells at each cross section. Thus, time-averaged concentrations were compared against final-time (12 years), down-gradient sulfate and chloride concentrations simulated over the corresponding monitoring well screen interval. Figures 5a-5b show that with the final calibrated model inputs, simulated concentrations fell within the range of measured values for all cross sections except GW008, the cross section farthest from reaching steady-state (see above). When the GW008 model is run to

18 years (Figures 6a), simulated concentrations reach the measured values (Figure 6b), providing some confidence in the calibration.

Major components of the flow model development consist of hydraulic property assignments. For each cross-section, a single hydraulic conductivity is assumed for each porous media type (fine tailings, coarse tailings and glacial till), which ignores heterogeneity. The fine and coarse tailings that make up the outer perimeter dike are man-made materials that likely exhibit relatively uniform properties, yet Table 3 shows that coarse tailing estimates based on field tests vary by an order of magnitude; averaged values applied for the tailings in the model do not represent this level of heterogeneity. Cross section-specific calibrated hydraulic conductivity addresses some of the extreme variability observed for the natural subsurface, glacial till, but any possible heterogeneity within a cross section is also ignored. Upscaled (averaged) parameters that are adequate for physical flow can often generate misleading results for solute transport, especially if they are chemically reactive [Harvey and Gorelick, 2000].

Unavailable up-gradient head measurements at the three west side cross-sections (GW006, GW007 and GW008) represents another noteworthy source of uncertainty. A nearby piezometer to the up-gradient end of the GW007 cross section provides some ground-based information for that cross section. The calibrated values for the other two cross sections rely on the assumption that the till hydraulic conductivity at GW007 approximates conditions for all of the west side, but this ignores the naturally variability noted in Table 3 and the differences in calibrated values for the three east side cross sections. Furthermore, calibration was based on observed down-gradient chloride concentrations, but up-gradient chloride concentration inputs used for the calibration were also uncertain (see below).

To address the absence of up-gradient sulfate and chloride measurements on the west side, average concentrations from Cell 2 on the east side of the basin were assumed. A single chloride concentration measurement taken at the piezometer near GW007 in September 2016 (T. Moe, personal communication, September 2016) fell within the range of measured values in Cell 2, lending some confidence in this approach.

The main check on the west side flow models are chloride concentrations and flux measured at Dark River [Kelly et al., 2016], which is a stream that drains the watershed containing the western part the Minntac basin. A reasonable assumption is that nearly all the chloride measured in the stream originates from the Minntac basin, because of very low natural background chloride conditions. We further assumed that all the chloride at the Dark River sampling site leaves the basin through groundwater flowing out of the western part of the basin, and that that total flow can be represented by flow through the three west side cross sections of GW006, GW007, and GW008. Observed chloride flux in Dark River then serves as another groundwater flow comparison for the west side models, in addition to chloride measured at monitoring wells for each cross section. To make the comparison, groundwater flux at GW006, GW007 and GW008 are averaged and converted to (volumetric) discharge by multiplying by an approximate cross sectional area below the entire western basin. The western basin cross section was calculated by the average (vertical) height of the GW006, GW007, and GW008 domains by the length of the perimeter dike corresponding to the western watershed (9672 m). Finally, multiplying the discharge by the up-gradient chloride concentration for the west side cross section results in $2.84 \times 10^8$ mg $Cl^-$/d. This is of the same order of magnitude but lower than the

measured rate of $6.64x10^8$ mg $Cl^-$/d at Dark River. Uncertainties in scaling up the modeled cross section fluxes include the assumption that the three cross sections apply to the entire western basin perimeter. Other possible sources of error are all those affecting the individual flux simulations for each of the cross sections.

To assess geochemical results with the model, simulated sulfate fluxes into and out of the cross sections were compared against estimates based on isotope data from the DNR [Kelly et al., 2016]. This comparison was made by normalizing all of the simulated sulfate fluxes by the total amount of sulfate added to the system (up-gradient cell water and recharge water). Figure 7 shows that, apart from MW12, DNR estimates of sulfate fluxes with recharge (dashed bars) compare relatively well with the model. DNR reduction estimates correlate well with simulated estimates for GW003, GW008, and MW12. Discrepancies between the studies for other cross sections could arise from uncertainty in the isotope-based estimates (see Kelly et al. [2016] for details) or model uncertainty in calibrated geochemical and hydraulic parameters. Simulated sulfate reduction are susceptible to uncertainty in kinetic decay parameters and organic carbon concentrations, which together directly control redox rates in the model. Simplifications in the geochemical model component include omitting major cations such as calcium and magnesium, which are known to sorb, and could thus influence iron concentrations and pH. Another simplification was the treatment of iron in the model, which includes only siderite (iron(II) carbonate mineral) and iron sulfide. Till sediments likely contain iron(III) minerals, which can compete with sulfate in redox reactions. Also, it is unknown how realistically siderite represents the iron reservoir for iron sulfide precipitation.

## Conclusions and Recommendations

The continued release of high concentrations of sulfate is an issue that requires continued attention, because sulfate can reduce to sulfide under anoxic conditions. Dissolved sulfide is toxic to wild rice (*Zizania palustris*) [MPCA, 2015], and sulfate reduction has also been associated with methyl mercury (MeHg) production [Branfireun et al. 1999; Harmon et al. 2004; Jeremiason et al. 2006], alkalinity increases, and phosphate release [Holmer and Storkholm, 2001].

A reactive transport model was implemented for 6 cross sections across the Minntac tailings basin's outer perimeter dike using hydrologic and geochemical observations as model inputs and calibration targets. Consistent with Kelly et al. (2016), simulations show that basin water serves as the largest sulfate source in nearly all the cross sections, but additional sulfate loading with recharge through the tailings material of the dike is also significant. Sulfate concentrations attenuate as groundwater leaves the dike, due to both dilution from recharge through naturally vegetated land and due to sulfate reduction. How much sulfate reduction occurs depends on organic carbon degradation rates and on groundwater velocities. However, in nearly all cross sections, the majority of sulfate leaves through out-flux at the down-gradient end rather than is reduced.

The biggest sources of uncertainty for the model consist of lack of data in the west side of the Minntac tailings basin, insufficient information about subsurface heterogeneity, and poor constraints on mechanisms controlling organic carbon degradation and sulfate reduction. To address these issues and improve our understanding of sulfate release from the Minntac tailings basin, we recommend the following additional data collection and model developments.

**Data recommendations**

Two recommendations for additional data are as follows:

(1) Install monitoring wells within the tailings basin on the western side.

These would enable direct hydrologic and geochemical observations that can replace currently inferred (and hence uncertain) model inputs. At a minimum, one west-side monitoring well should be established; pre-existing wells on the west side could be brought back into service for this (e.g., the within-perimeter wells near GW007). However, if possible, we recommend 3 within-basin wells collocated with outside monitoring wells (GW006-GW008), because unlike well-mixed surface water sources on the east-side, up-gradient subsurface conditions on the west-side may vary spatially and require multiple monitoring points.

Measurements at the additional within-basin wells should be coordinated with measurements at outside wells to provide information at comparable time frequencies. Water-level measurements at the wells should be taken to help constrain groundwater flow, and the standard suite of water chemistry analytes and parameters (dissolved ion concentrations, pH, alkalinity, and temperature) should be measured to provide up-gradient geochemical model inputs.

(2) Collect cores of the subsurface material across the perimeter dike to analyze hydraulic, geochemical, and microbial properties.

Previous cores taken within the Minntac basin cannot be assumed to represent varying hydraulic and geochemical conditions through the cross-sections, which include different tailings materials and naturally heterogeneous underlying till. Representative dike cores should be located on both the western and eastern sides of the basin. A series of two to three cores traversing the dike on either side of the basin would help capture spatial heterogeneity within a cross-section. On the west-side, core collection could be coordinated with drilling of new within-basin wells (as recommended above).

With core sediments, we recommend physical measurements such as grain-size to help constrain spatially heterogeneous hydraulic conductivities, which can replace current uniform values (within a certain material type) that are inadequate given ranges previously found (Table 3). Geochemical measurements should include iron sulfide sediment extractions to confirm its formation, which has until now only been inferred from water chemistry and model simulations. Organic carbon extractions from till should be carried out to constrain its degradation and associated sulfate reduction. If possible, pore water samples could be taken, yet its procedural challenges and limited representation of transient conditions make this a lower priority analysis.

The final recommended analysis is for lab experiments with till sediments to measure anaerobic degradation rates (associated with sulfate reduction). This requires specialized laboratory resources and may differ from field-scale rates, but it would offer valuable direct information about reaction rates, which are critical for predictive modeling capabilities.

**Model development recommendations**

Some of the further geochemical model developments needed for improving simulations of sulfate release depend on the recommended new data, specifically greater details on the mechanisms controlling organic carbon degradation and coupled sulfate reduction. Other improvements can be made using available water chemistry data. As the first reactive-transport modeling effort to represent groundwater sulfate at a tailings basin on the Iron Range, our study simplified the geochemical conceptual model in order to develop the general framework. In particular, major cations such as calcium and magnesium were omitted from the model, even though water chemistry measurements have shown their concentrations to vary spatially, suggesting that they may serve as indicators for preferential flow paths or redox-related geochemical activity. Cations such as calcium and magnesium are commonly mobilized by cation exchange; we thus recommend that the next step in the geochemical model development should include incorporating calcium and magnesium as cation exchanging species. A related recommendation would be to test alternative sources of iron that is available for iron sulfide precipitation. The model currently represents this reservoir as siderite, but another possibility is sorbed ferrous iron, which could have distinct reaction properties and geochemical impacts from siderite.

Before the reactive transport models should be implemented for future scenario predictions, rigorous uncertainty quantification is needed. Figures showing goodness-of-fit with target calibration data (Figures 5a-5b and 6b) provide graphical information, but these need to be converted to uncertainty ranges in the corresponding calibrated parameters. Future scenarios can then be tested using parameter values within these ranges, in order to properly demonstrate uncertainty in the model and avoid over-confidence in their predictions into the future.

Improving the characterization of sulfate release from the Minntac tailings basin (and other similar settings in Minnesota) requires continued and new monitoring and additional model development and application. Reactive-transport models can play a critical role in evaluating future scenarios of sulfate release as Minntac's activities move forward and as site closure is planned, but a greater understanding of geochemical mechanisms and subsurface physical properties is first needed to reliably project sulfate reduction processes long into the future.

## References


Bavin, T., Koski, S., Jacobs, C., Berndt, M., and Kelly, M. (2016), Physical and Hydrologic Properties of Taconite Tailings. Minnesota Department of Natural Resources Research Report, Division of Lands and Minerals, St. Paul, MN, 50 p.

Bear, J. and A. Verruijt. (1987). Modeling Groundwater Flow and Pollution. D. Reidel Publishing Co., Netherlands de Marsily, G. 1986. *Quantitative Hydrogeology,* Academic Press, San Diego.

Berndt, M., Bavin, T., and Kelly, M., (2016a), Geochemical tracer based (GTB) sulfate balance models for active tailings basins on Minnesota's Iron Range (I) process waters. Minnesota Department of Natural Resources Research Report, Division of Lands and Minerals, St. Paul, MN, 60 pages.

Berndt, M., Bavin, T., Koski, S., Jacobs, C., and Kelly, M., (2016b), Geochemical tracer based (GTB) sulfate balance models for active tailing basins on Minnesota's Iron Range (II) pore waters. Minnesota Department of Natural Resources Research Report, Division of Lands and Minerals, St. Paul, MN, 51 pages.

Branfireun, B. A., Roulet, N. T., Kelly, C., & Rudd, J. W. (1999). In situ sulphate stimulation of mercury methylation in a boreal peatland: Toward a link between acid rain and methylmercury contamination in remote environments.*Global Biogeochemical Cycles*, 13(3), 743-750.

CRA (Conestoga-Rovers and Associates) (2013), Groundwater Flow and Sulfate Transport Modeling Report, Minntac Tailings Basin, U.S. Steel Corporation, Mountain Iron, MN, Conestoga-Rovers and Associates, Saint Paul, MN

DNR (Minnesota Department of Natural Resources) (2016), MnTOPO, *Arcgis.dnr.state.mn.us*. Available from: http://arcgis.dnr.state.mn.us/maps/mntopo/ (Accessed 2 October 2016)

Garabedian, S.P., LeBlanc, D.R., Gelhar, L.W., and Celia, M.A. (1991), Large-scale natural-gradient tracer test in sand and gravel, Cape Cod, Massachusetts: 2. Analysis of spatial moments for a nonreactive tracer. *Water Resour. Res.,* 27(5), 911-924.

Gelhar, L. W., C. Welty, and K.W. Rehfeldt, (1992), A critical review of data on field-scale dispersion in aquifers,*Water Resour. Res.,* 19(1), 161 – 189

Harbaugh, A. W. (2005), MODFLOW-2005, the U.S. Geological Survey modular ground-water model – the Ground-Water Flow Process: U.S. Geological

Harmon, S. M., King, J. K., Gladden, J. B., Chandler, G. T., & Newman, L. A. (2004). Methylmercury science & technology, 38(2), 650-656.

Harvey, C., and Gorelick, S. M. (2000), Rate - Wilted mass transfer or
dominates plume evolution at the macrodispersion experiment (MADE) site?. *Water Resources Research, 36*(3), 637-650.

Holmer, M. ., & Storkholm, P. . (2001). Sulphate reduction and sulphur cycling in lake sediments: a review. *Freshwater Biology*, *46*, 431–451. http://doi.org/10.1046/j.1365-2427.2001.00687.x

Jakobsen, R., and D. Postma (1999), Redox zoning, rates of sulfate reduction and interactions with Fe-reduction and methanogenesis in a shallow sandy aquifer, Rømø, Denmark, *Geochim. Cosmochim. Acta*, 63(1), 137–151.

Jeremiason, J. D., Engstrom, D. R., Swain, E. B., Nater, E. A., Johnson, B. M., Almendinger, J. E., Monson, B. A., & Kolka, R. K. (2006). Sulfate addition increases methylmercury production in an experimental wetland. *Environmental science & technology*, 40(12), 3800-3806.

Kelly, M., Berndt M., Bavin, T. and Koski, S., (2016), Geochemical Tracer Based (GTB) Sulfate Balance Models (III) Well waters, seeps, and downstream surface waters. Minnesota Department of Natural Resources Research Report, Division of Lands and Minerals, St. Paul, MN, 60 p.

Li, Y. H. and S. Gregory. 1974. Diffusion of ions in seawater and in deep-sea sediments. *Geochimica et Cosmochimica Acta*, *38, 703 - 714.*

MGS (Minnesota Geological Survey) (2016), State Geology Data: Minnesota, *Mngeo.state.mn.us*. Available from: http://www.mngeo.state.mn.us/chouse/geology/statewide.html (Accessed 2 October 2016)

MPCA (Minnesota Pollution Control Agency) (2015), Draft proposal to protect wild rice from excess sulfate. March 24, 2015. wq-s6-43k.

Parkhurst, D. L., and C. A. J. Appelo (1999), User's guide to PHREEQC: A computer program for speciation, reaction-path, ID-transport, and inverse geochemical calculations, *U.S. Geol. Surv. Water Resour. Invest. Rep.*, 99–4259, 312 p.

Prommer, H., D. A. Barry, and C. Zheng (2003), MODFLOW/MT3DMS-based reactive multicomponent transport modeling, *Ground Water*, 41, 247–257, doi:10.1111/j.1745–6584.2003.tb02588.x.

STS Consultants Ltd (STS) (2007), Subsurface Exploration and Seepage Evaluation, Minntac Tailings Basin, Mountain Iron, MN, U.S. Steel Corporation, STS Consultants Ltd, Vernon Hills, IL

USS (U.S. Steel) (1987), Final NPDES Permit # MN 0057207, Minntac Tailings Basin Area, MT. Iron, Minnesota, Hydrogeologic Report,U.S. Steel, Mt Iron, MN

Zheng, C., and P. P. Wang (1999), MT3DMS: A modular three-dimensional multispecies model for simulation of advection, dispersion and chemical reactions of contaminants in groundwater systems: Documentation and user's guide,Contract Rep. SERDP-99-1, U.S. Army Eng. Res. and Dev. Cent., Vicksburg, Miss.

## Tables and Figures

*Table 1: Domain length and up-gradient and down-gradient head values (based on Lake Superior Datum) for all cross-sections [M. Kelly, personal communication, July 2015, T. Moe, personal communication, Sept 2016] Calibrated hydraulic conductivities for all cross-sections are listed. Averaged hydraulic conductivities for fine and coarse tailings were taken from slug tests conducted by [STS, 2007]. *Calibrated values.*

| Cross-Section | Domain Length (m) | Up-Gradient Head (m) | Down-Gradient Head (m) | Glacial Till Hydraulic Conductivity (m/d) |
|---|---|---|---|---|
| **EAST** | | | | |
| GW003 | 224 | 270.2 | 262.2 | 2.46 (glacial till) |
| GW004 | 213.4 | 269.4 | 265.8 | 2.4 (glacial till) |
| MW12 | 342.9 | 269.4 | 258.9 | 1.6 (glacial till) |
| **WEST** | | | | |
| GW006 | 170 | 271.3* | 261.9 | 0.56 (glacial till) |
| GW007 | 177 | 264.8 | 257.7 | 0.56 (glacial till) |
| GW008 | 220 | 276.9* | 267.8 | 0.56 (glacial till) |
| **Perimeter Dike** | | | | |
| Coarse Tailings | N/A | N/A | N/A | 0.672 |
| Fine Tailings | N/A | N/A | N/A | 0.033 |

*Table 2: Recharge rates taken from MNDNR report [Bavin, 2016].*

| Recharge Location | Recharge Rate (m/d) |
|---|---|
| Perimeter Dike | 0.00084 |
| Natural Land Surface | 0.00056 |

*Table 3: Range of hydraulic conductivity values taken from slug tests conducted by [STS, 2007] as well as slug and pumping tests conducted by [CRA. 2013].*

| Subsurface Material | Range of Observed Hydraulic Conductivity (m/d) |
|---|---|
| Coarse Tailings | 0.137 - 1.527 |
| Fine Tailings | 0.032 - 0.034 |
| Glacial Till | 0.021 - 13.870 |

*Table 4: Values used for each cross-section. Temperature and pH values taken from averaged measured values over time for each respective monitoring well [Kelly et al., 2016]*

| **Cross-Section** | **Temperature (°C)** |
|---|---|
| **EAST** | |
| GW003 | 9.14 |
| GW004 | 6.25 |
| MW12 | 5.34 |
| **WEST** | |
| GW006 | 11.39 |
| GW007 | 7.63 |
| GW008 | 7.91 |

*Table 5: Values for up-gradient concentrations. Concentrations were taken from averaged measured values from Cell 1 for GW003 and Cell 2 for the remaining cross-sections [Kelly et al., 2016].*

| **Cross-Section** | **Up-Gradient Initial Value SO4 (mg/L)** | **Up-Gradient Initial Value Cl (mg/L)** |
|---|---|---|
| **EAST** | | |
| GW003 | 907.24 | 147.57 |
| GW004 | 925.67 | 141.557 |
| MW12 | 925.67 | 141.557 |
| **WEST** | | |
| GW006 | 925.67 | 141.557 |
| GW007 | 925.67 | 141.557 |
| GW008 | 925.67 | 141.557 |

*Table 6: Initial concentrations for the model domain, equilibrated with siderite and charge-balanced (with adjustments to sodium) using PHREEQC.*

| **Aqueous Species** | **Initial Porewater Concentrations** |
|---|---|
| Inorganic Carbon (M) | 3.50E-02 |
| Chloride (M) | 0 |
| Iron (M) | 2.30E-05 |
| Sodium (M) | 2.80E-03 |
| Sulfate (M) | 7.80E-09 |
| Dissolved Oxygen (M) | 0 |
| pH | 7.1 |

*Table 7: Organic carbon concentrations set within the glacial till for each cross-section. Organic carbon was adjusted to control reduction of sulfate in order to have modeled monitoring well concentrations match measured concentrations. Concentrations are moles per liter of water.*

| **Monitoring Well** | **Organic Carbon in Model (mol/Lw)** |
|---|---|
| **EAST** | |
| GW003 | 0.00066 |
| GW004 | 0.00101 |
| MW12 | 0.00047 |
| **WEST** | |
| GW006 | 0.000021 |
| GW007 | 0.000021 |
| GW008 | 0.00061 |

*Table 8. Water balance discrepancies calculated by MODFLOW for steady-state flow simulations for each cross-section.*

| x-section | Water Balance Discrepancy (%) |
|---|---|
| GW003 | -0.01 |
| GW004 | -0.13 |
| GW006 | 0.04 |
| GW007 | 1.19 |
| GW008 | 0.02 |
| MW12 | -0.01 |

*Table 9. Solute mass balance discrepancies calculated by PHT3D at the end of the 12-year model simulation for each cross-section.*

| Species | GW003 discrepancy (%) | GW004 discrepancy (%) | GW006 discrepancy (%) | GW007 discrepancy (%) | GW008 discrepancy (%) | MW12 discrepancy (%) |
|---|---|---|---|---|---|---|
| C(4) | 0.74 | 0.49 | 0.09 | 1.53 | -0.38 | 0.41 |
| Cl | 2.68 | 0.73 | 0.24 | 2.52 | -4.56 | 0.81 |
| Fe(2) | -0.22 | -0.19 | -0.32 | -0.41 | -0.32 | 0.08 |
| Na | 0.96 | 0.16 | 0.17 | 1.52 | 2.03 | 1.18 |
| O(0) | -0.23 | -0.47 | 0.05 | 0.45 | 0.02 | -0.20 |
| S(-2) | 0.58 | 0.47 | 0.00 | 0.17 | -0.49 | 0.33 |
| S(6) | 0.36 | -0.26 | 0.18 | 1.25 | 2.33 | 0.95 |

*Table 10. Simulated sulfate flux into and out of the cross sectional domains, calculated for the final 0.1 years (36.5 days) simulated. Sources of sulfate are listed in blue, while sinks are in yellow. Total In is the sum of the up-gradient flux and the recharge flux. Total Out is the sum of down-gradient flux out and reduction out; Precipitation Out represents a portion of Reduction Out. Units are molar rate [kmol S/yr] per unit aquifer thickness (in the direction perpendicular to the cross-section) [m].*

| **Simulated $SO_4$ fluxes [kmol S / (yr*m)]** | | | | | | |
|---|---|---|---|---|---|---|
| | **GW003** | **GW004** | **MW12** | **GW006** | **GW007** | **GW008** |
| Up-gradient In | 4.31 | 1.95 | 0.91 | 1.17 | 0.89 | 0.26 |
| Recharge In | 0.69 | 0.62 | 0.59 | 0.51 | 0.53 | 0.51 |
| ***TOTAL IN*** | ***5.01*** | ***2.57*** | ***1.49*** | ***1.68*** | ***1.42*** | ***0.77*** |
| Down-gradient Out | 4.03 | 1.11 | 0.89 | 1.68 | 1.33 | 0.25 |
| Reduction Out | 0.91 | 1.34 | 0.52 | 0.00 | 0.00 | 0.34 |
| ***TOTAL OUT*** | ***4.94*** | ***2.45*** | ***1.41*** | ***1.68*** | ***1.33*** | ***0.59*** |
| Precipitation Out | 0.55 | 0.92 | 0.22 | 0.00 | 0.00 | 0.33 |

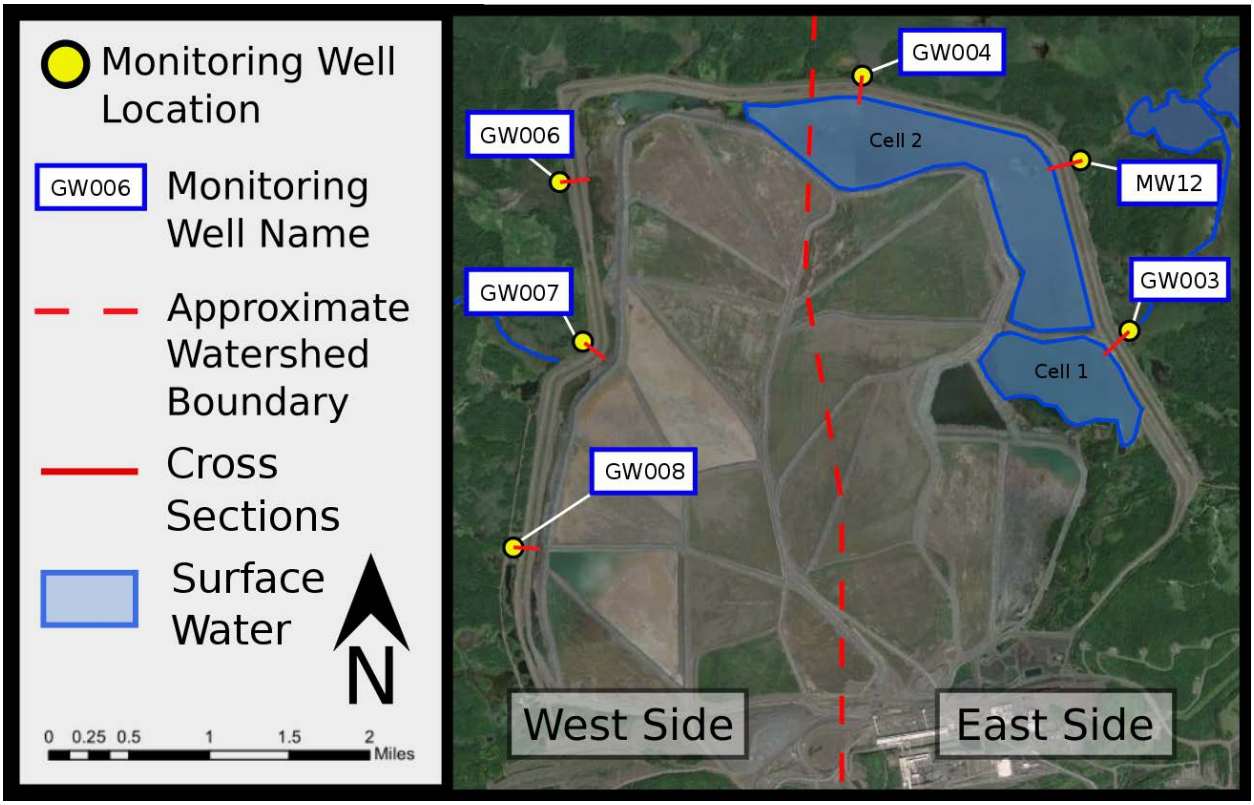


*Figure 1: Mapview of Minntac Tailings Basin.*

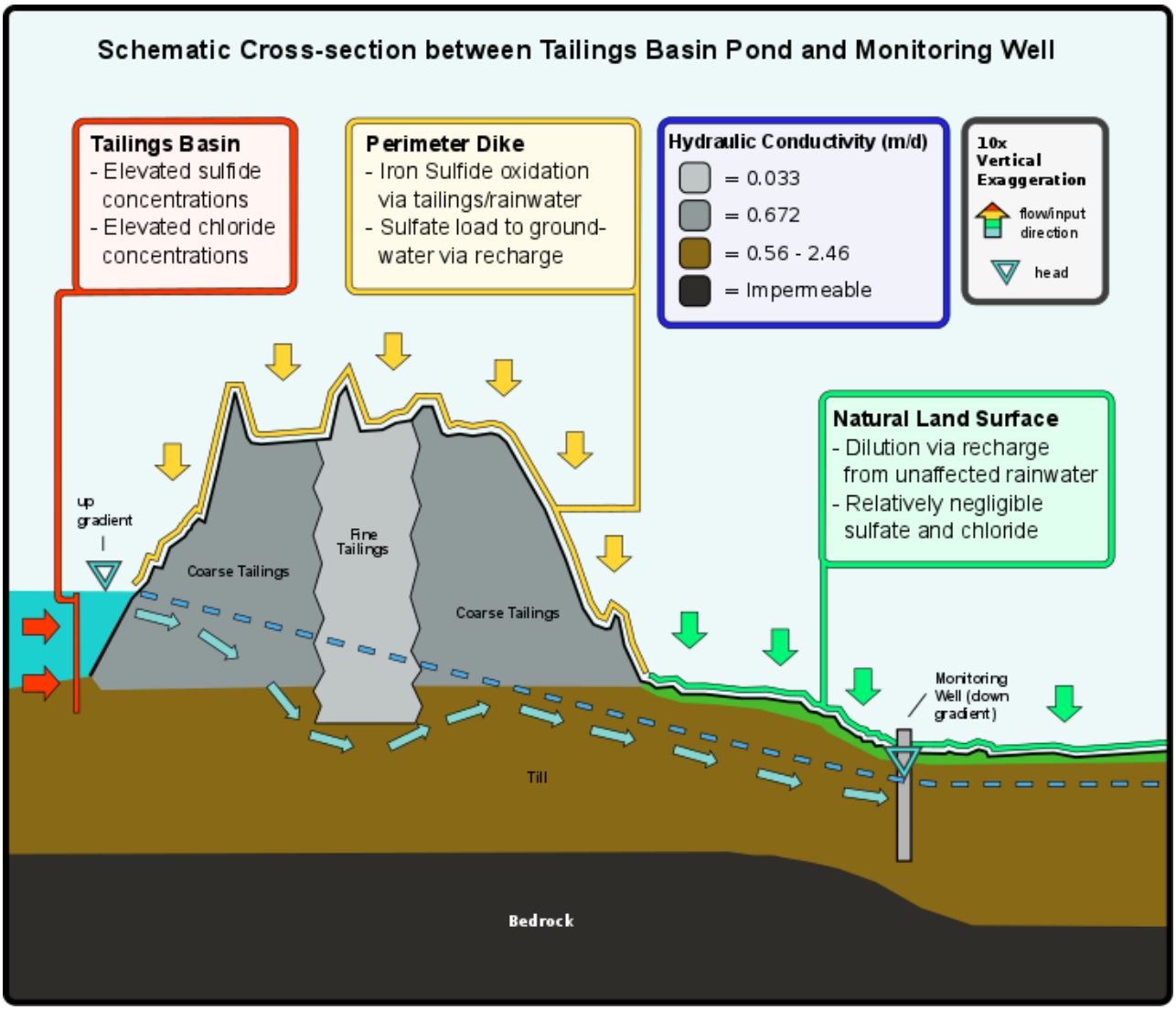


*Figure 2: Schematic of cross-section.*

# East Side

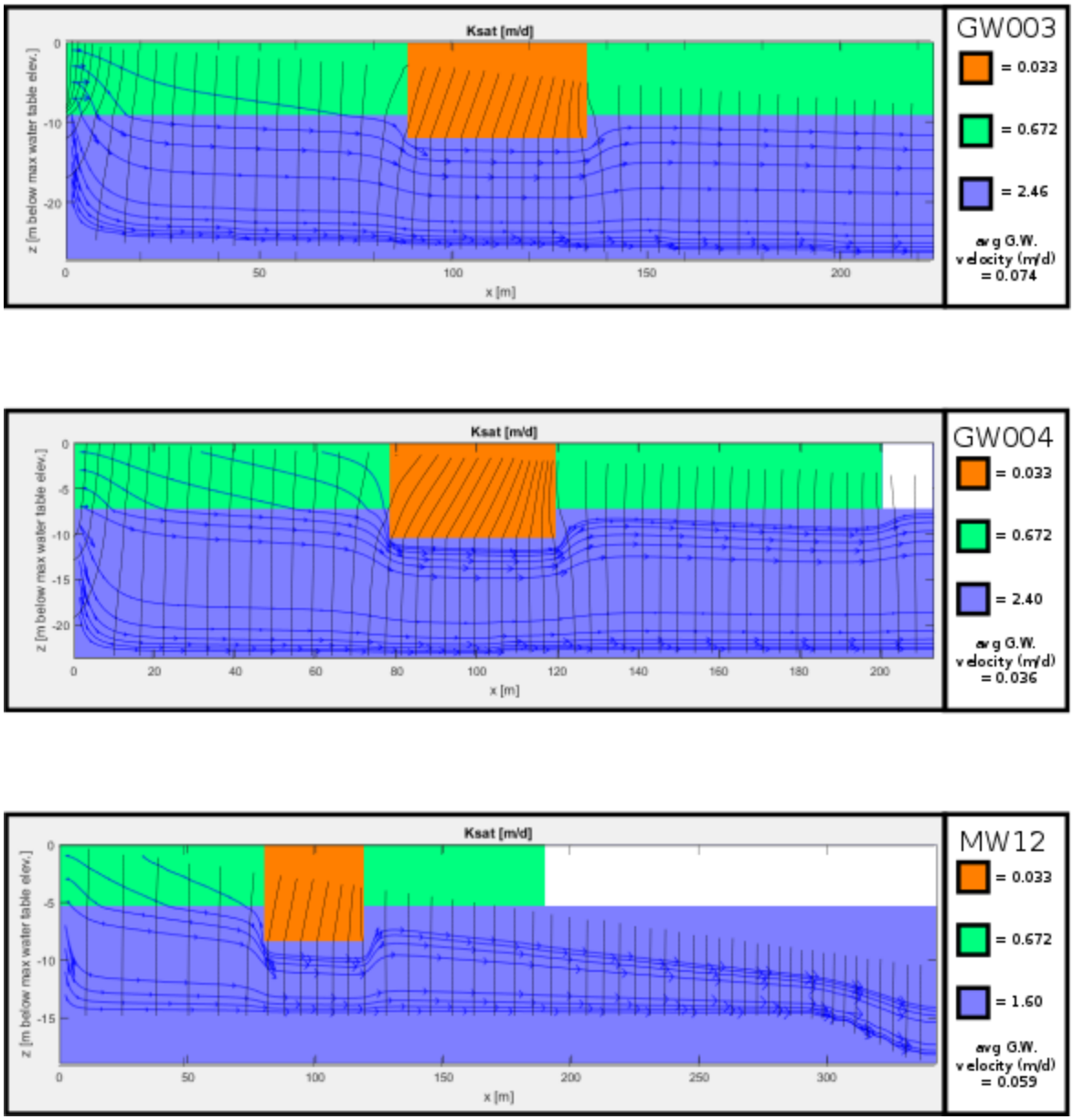


*Figure 3a: Cross-sections of the three transects on the east side of the tailings basin. Hydraulic conductivity (m/d) are listed for the fine tailings inner core (orange), the coarse tailings outer core (green), and the the underlying glacial till (light blue). The black lines are head contours (equipotential lines), and the dark blue lines represent the flow paths. White areas designate the air above the cross-section. No flow boundary conditions exist along the bottom of each cross-section, fixed head boundaries are set at both the left and right boundaries, recharge (flux) conditions are set at the top of each cross-section (with distinct recharge rates above the perimeter dike and above the natural land surface).*

# West Side

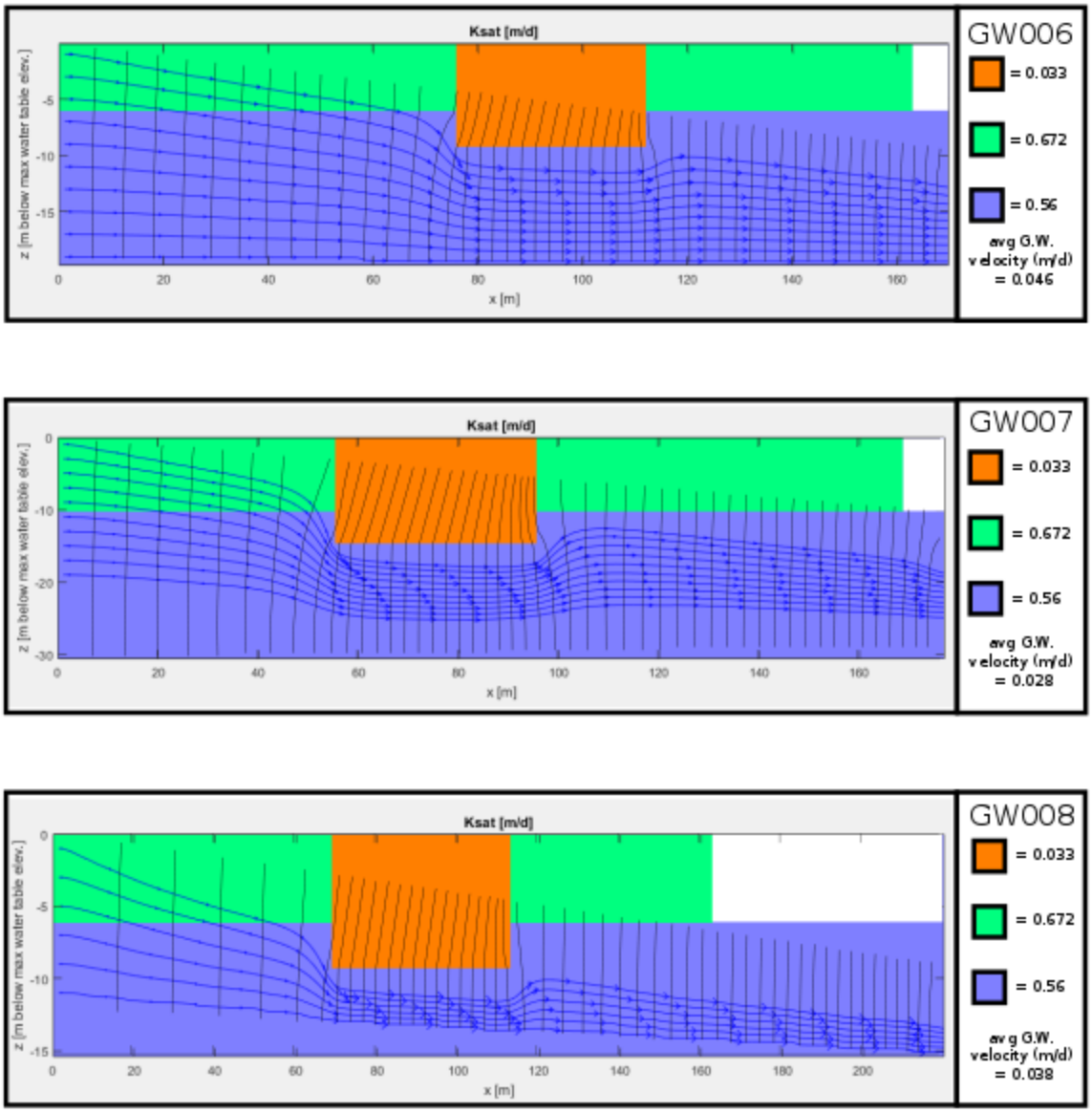


*Figure 3b: Cross-sections of the three transects on the west side of the tailings basin. Hydraulic conductivity (m/d) are listed for the fine tailings inner core (orange), the coarse tailings outer core (green), and the the underlying glacial till (light blue). The black lines are head contours (equipotential lines), and the dark blue lines represent the flow paths. White areas designate the air above the cross-section. No flow boundary conditions exist along the bottom of each cross-section, fixed head boundaries are set at both the left and right boundaries, recharge (flux) conditions are set at the top of each cross-section (with distinct recharge rates above the perimeter dike and above the natural land surface).*

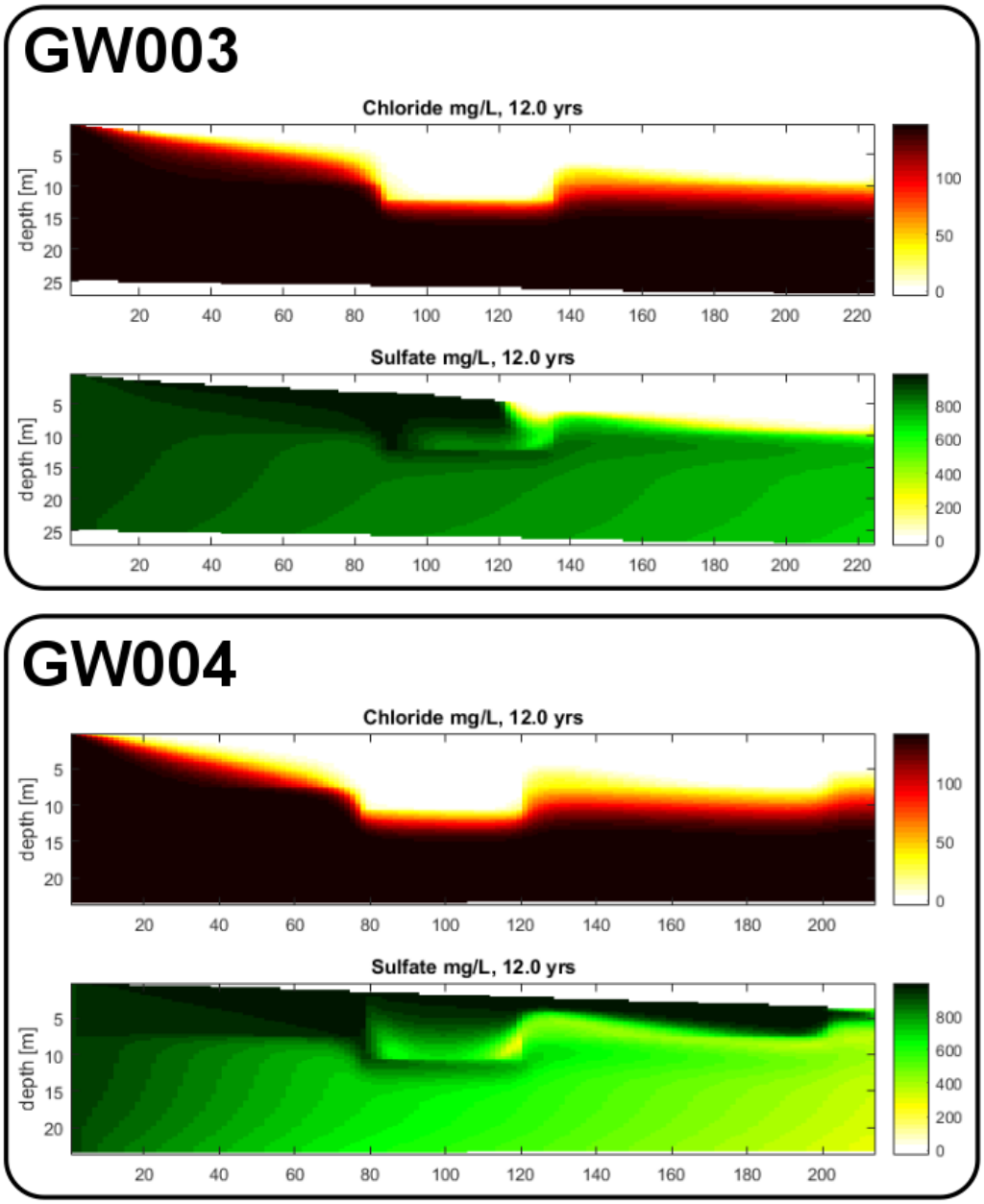


*Figure 4a: Cross-sections GW003 and GW004 run for twelve years. Upper plot depicts chloride concentrations, lower plot depicts sulfate concentrations. The horizontal extent is in meters.*

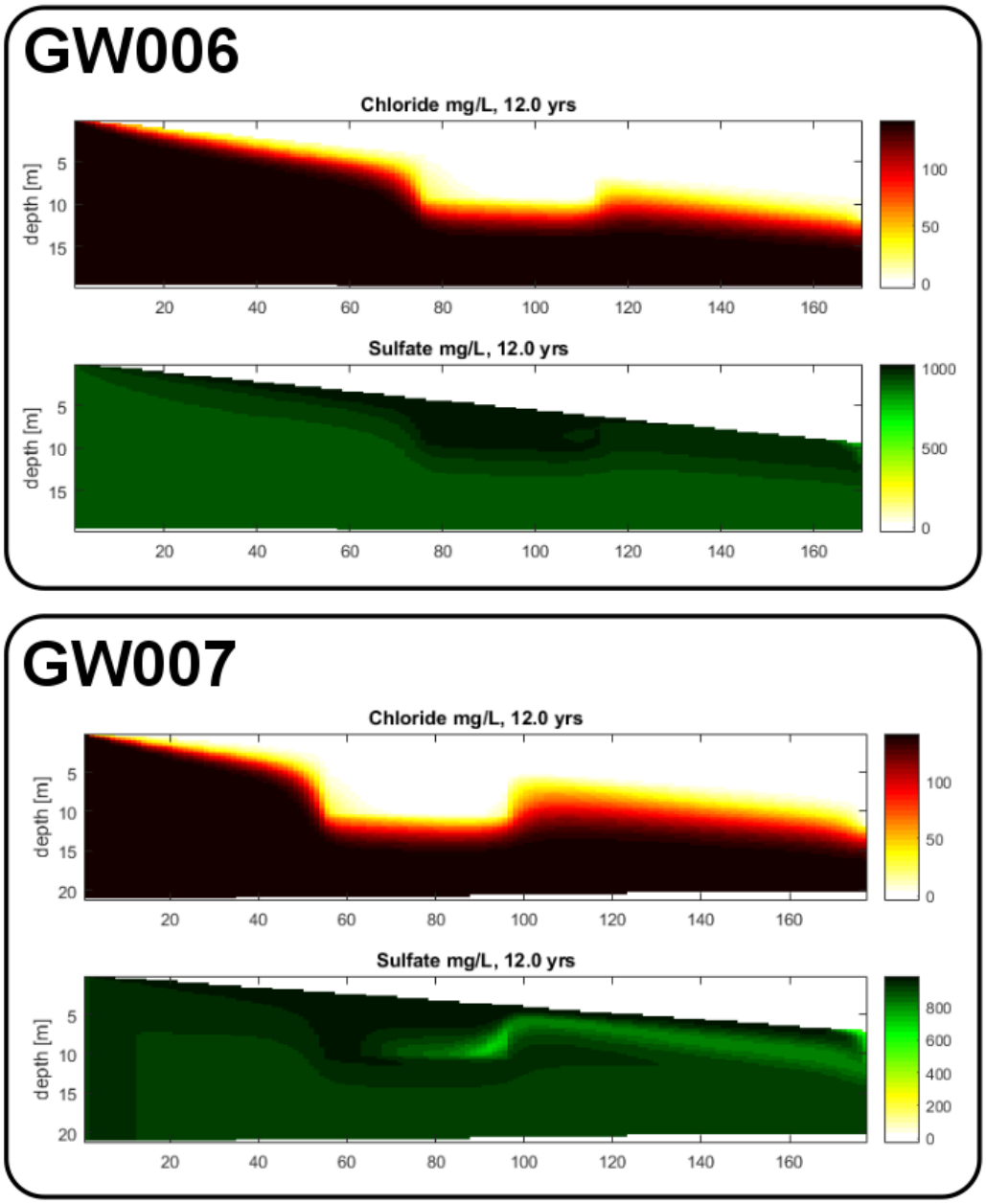


*Figure 4b: Cross-sections GW006 and GW007 run for twelve years. Upper plot depicts chloride concentrations, lower plot depicts sulfate concentrations. The horizontal extent is in meters.*

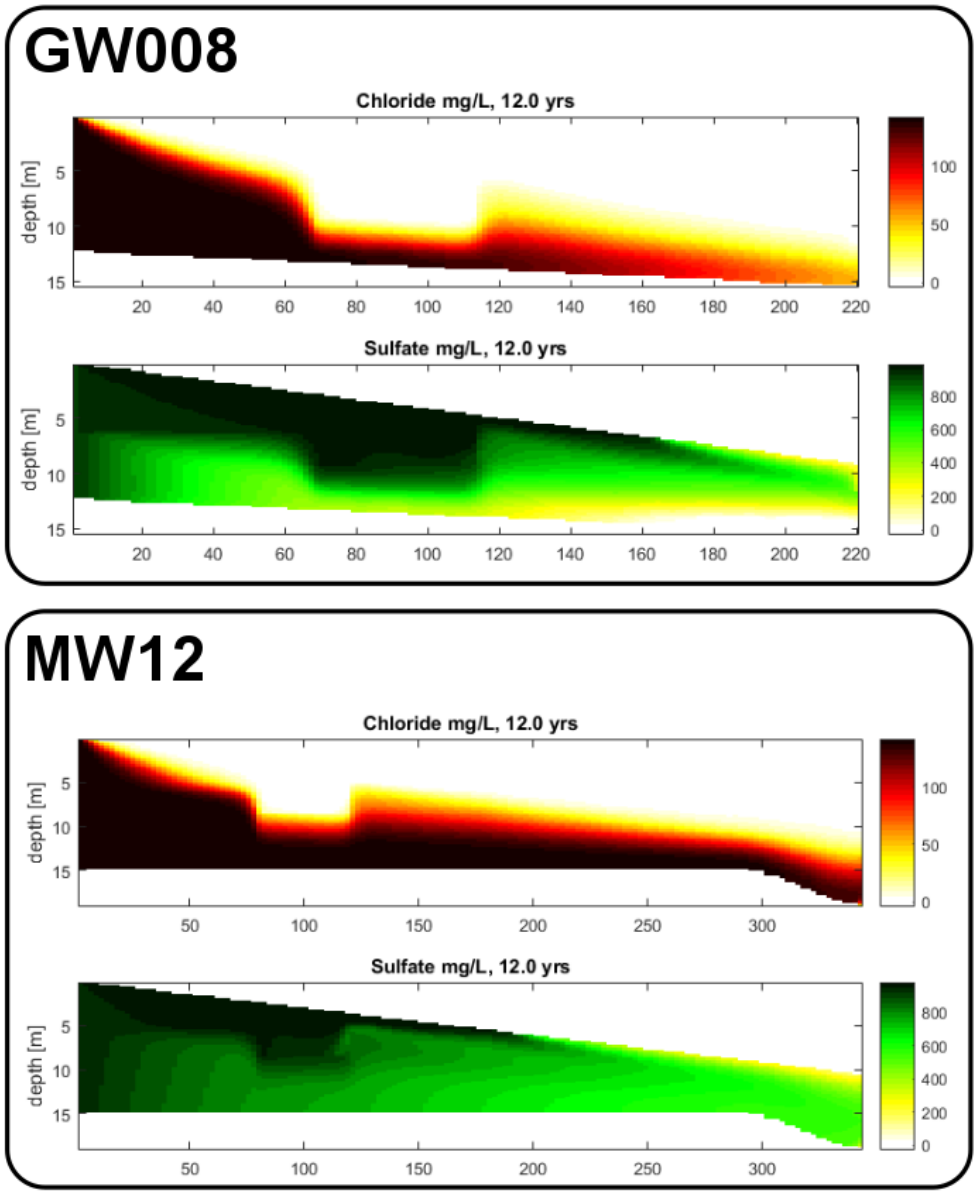


*Figure 4c: Cross-sections GW008 and MW12 run for twelve years. Upper plot depicts chloride concentrations, lower plot depicts sulfate concentrations. The horizontal extent is in meters.*

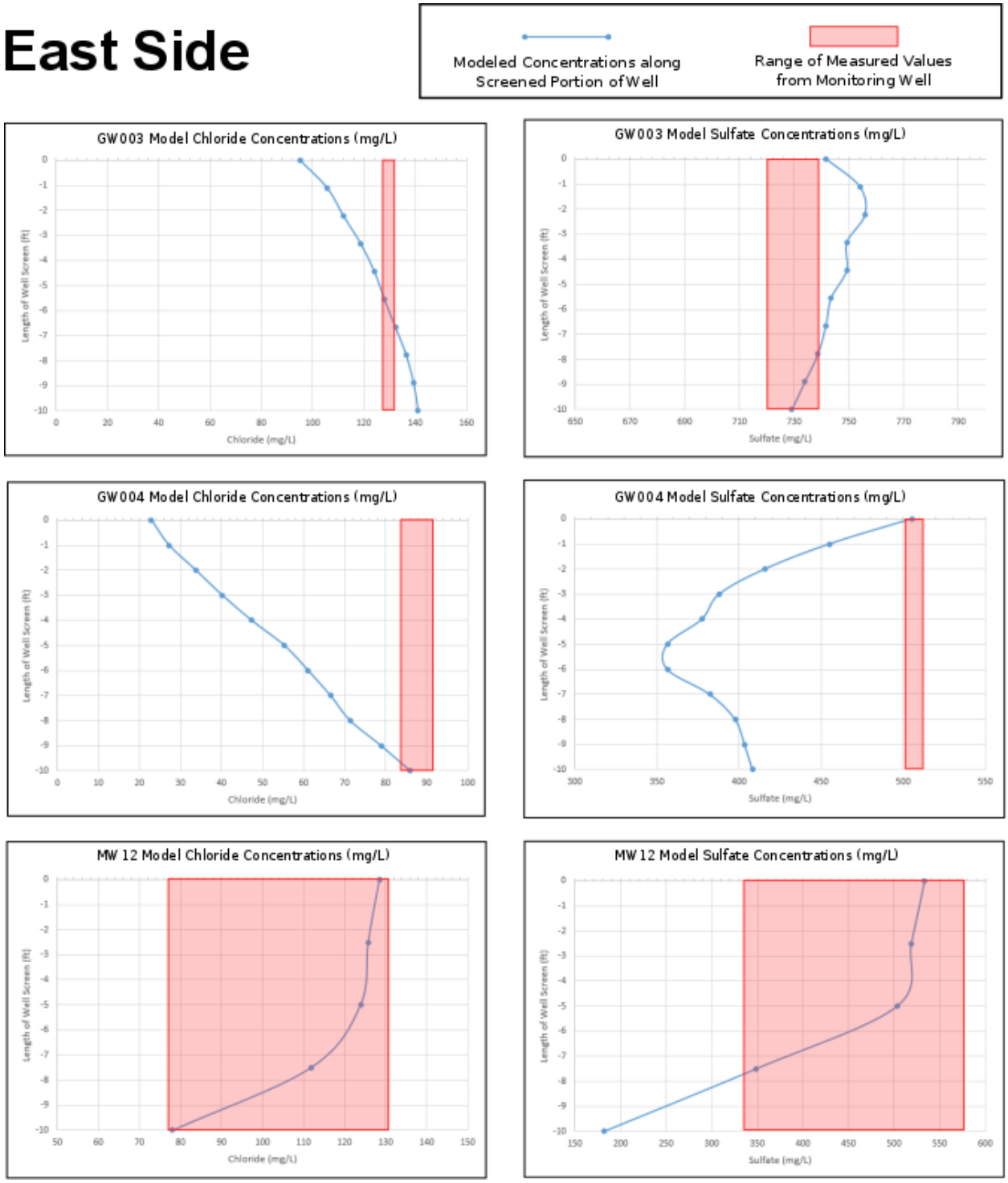


*Figure 5a: East side concentrations. The blue lines represent modeled concentrations along the length of the screened portion of each monitoring well. The red boxes represent ranges of measured concentrations. All units are in mg/L.*

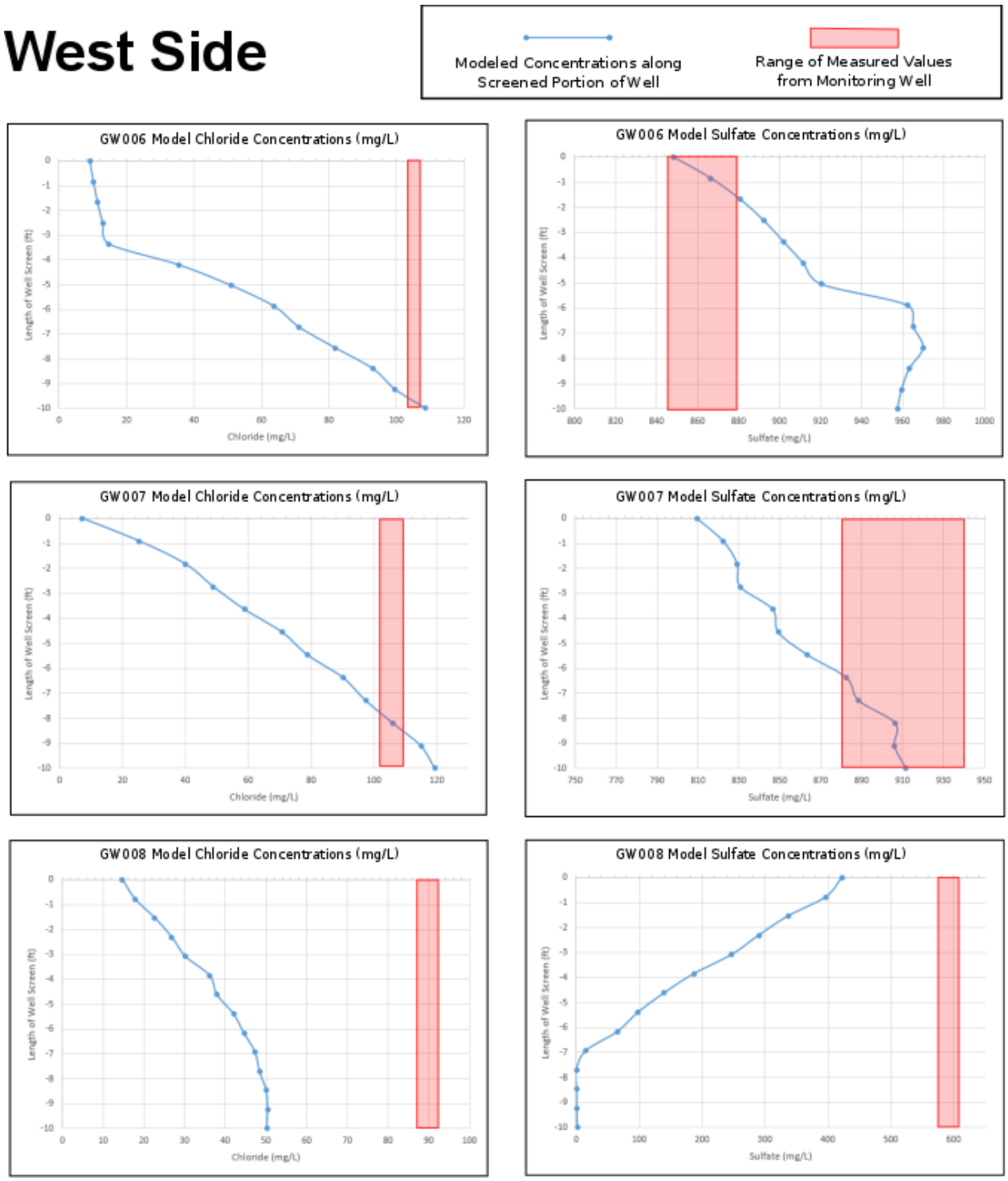


*Figure 5b: West side concentrations. The blue lines represent modeled concentrations along the length of the screened portion of each monitoring well. The red boxes represent ranges of measured concentrations. All units are in mg/L.*

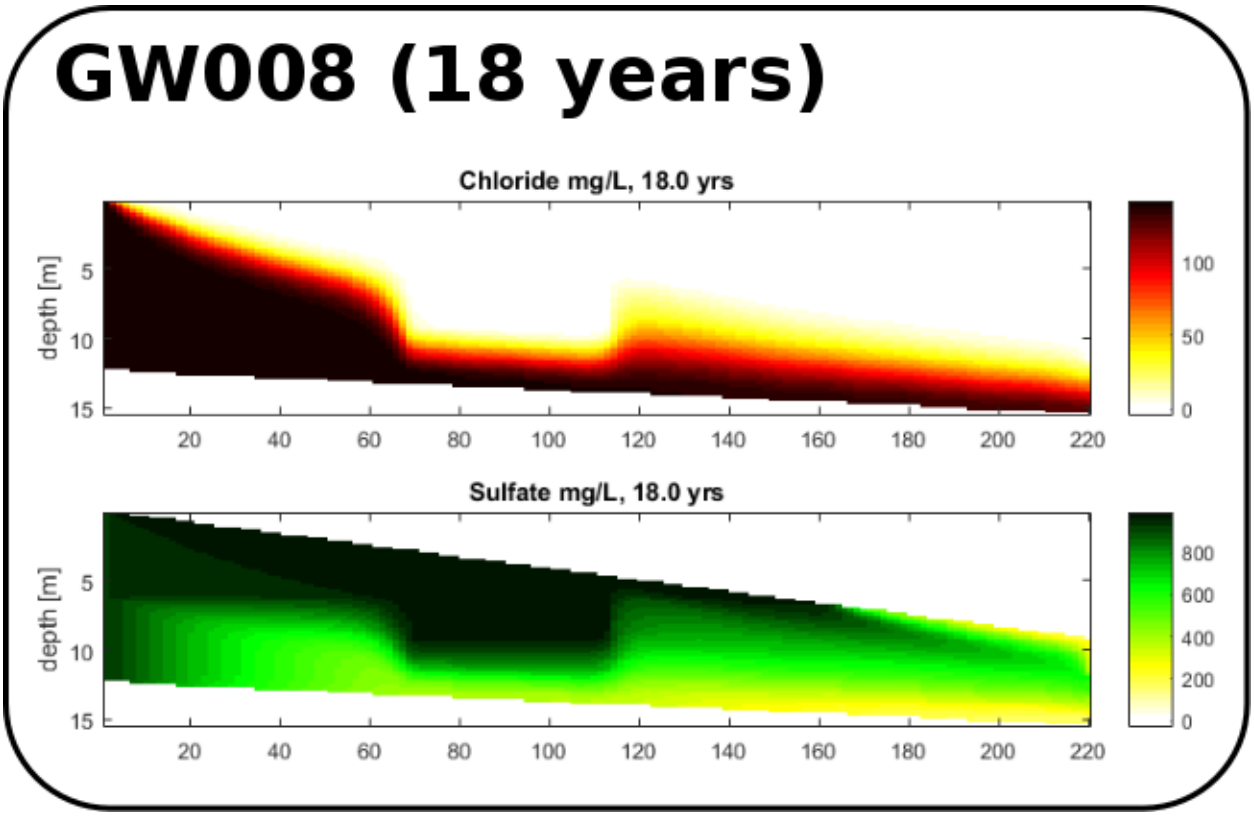


*Figure 6a: Cross-sections GW008 run for eighteen years. Upper plot depicts chloride concentrations, lower plot depicts sulfate concentrations. The horizontal extent is in meters.*

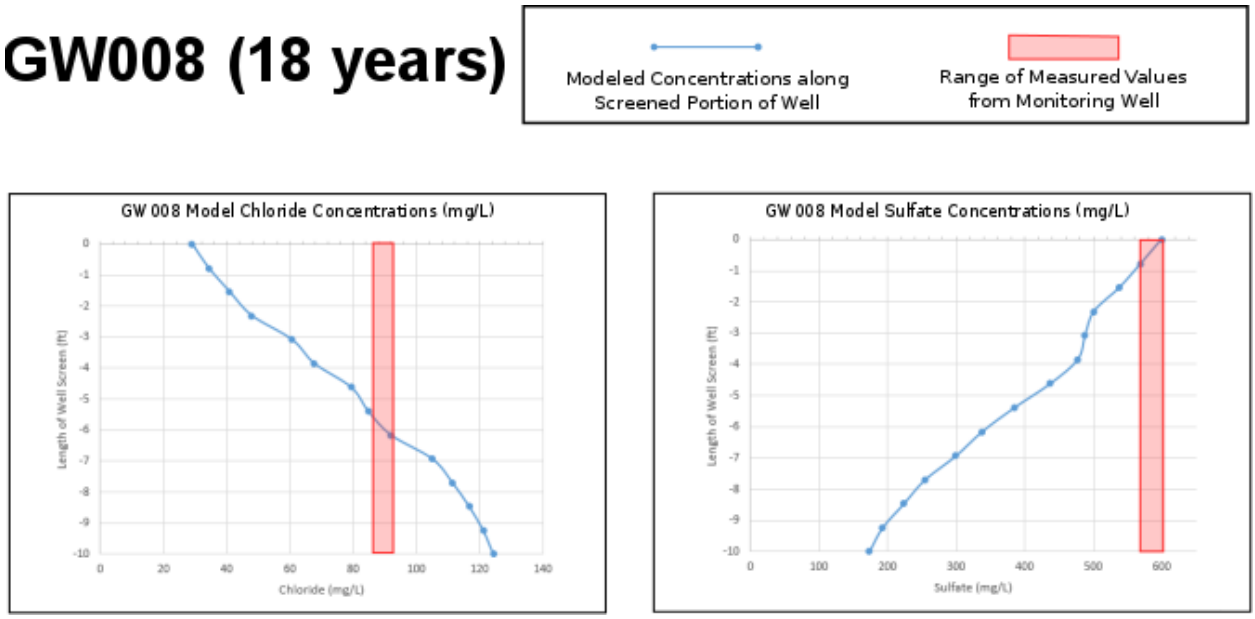


*Figure 6b: West side concentrations. The blue lines represent modeled concentrations along the length of the screened portion of each monitoring well. The red boxes represent ranges of measured concentrations. All units are in mg/L.*

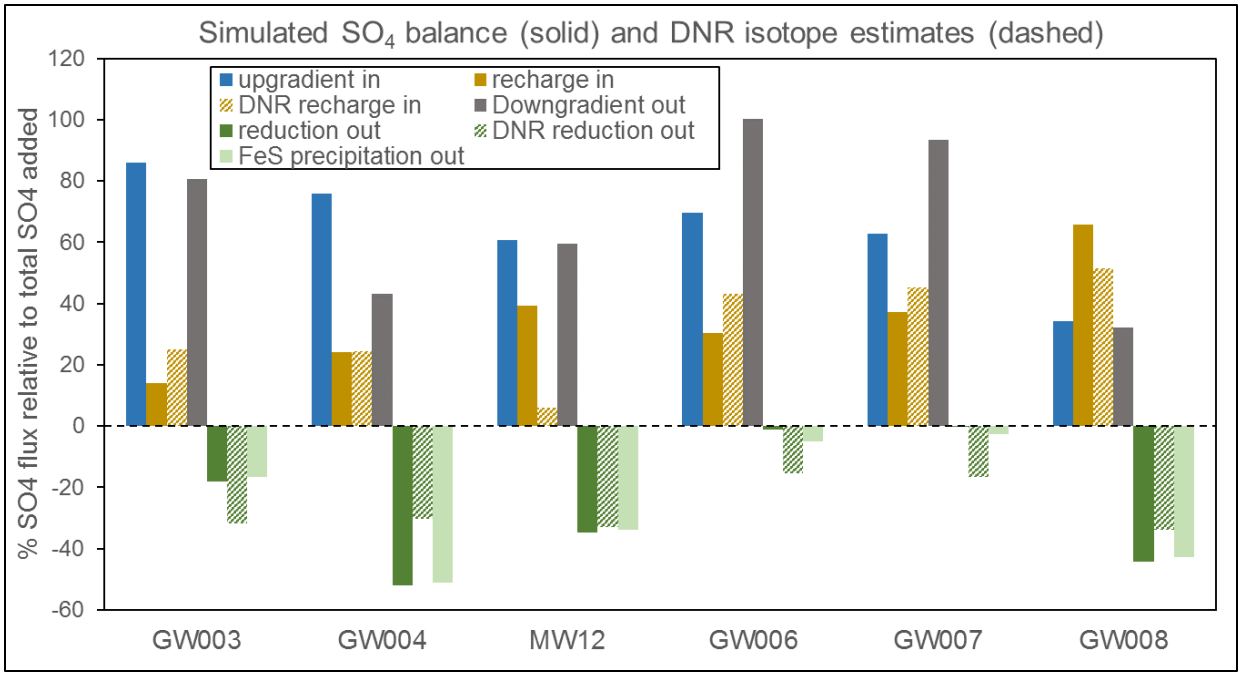


*Figure 7: Comparison of simulated flux percentages (solid bars) with DNR estimates (dashed bars) based on isotope data (Kelly et al., 2016). Both data sources are normalized by the total SO4 flux into the system (up-gradient cell water + recharge).*